Nanorotors

International Edition: DOI: 10.1002/anie.201509108
German Edition: DOI: 10.1002/ange.201509108

Conformational Slippage Determines Rotational Frequency in Five-Component Nanorotors

*Soumen K. Samanta[+], Anup Rana[+], and Michael Schmittel**

Dedicated to Professor H. Günther on the occasion of his 80th birthday

Abstract: *Several five-component nanorotors ROT-3 that rotate at different rates were prepared by adding phenanthrolines of distinct lateral size as brake blocks to the four-component nanorotor ROT-2. The brake blocks interfere with the 180° rotor causing the rotational frequency to drop from 97 kHz to 5 kHz. The effect of the rotating brake blocks on the rotational frequency in ROT-3 is accurately predicted by a nanomechanical model called "conformational slippage". For quantification, the interaction of the brake blocks with the trajectory of the main rotator is gauged based on the number of interfering vs. non-interfering conformations as computed by PM6.*

Numerous biological machines (kinesin motor proteins,[1a] ATP synthase,[1b] and bacterial flagella)[1d] are in essence sophisticated multicomponent heteroaggregates, which maintain essential life processes through astonishing nanomechanical movements.[1] For example, the rotation rate of the naturally occurring bacterial flagellar motor[1d,2] decreases depending on the concentration of cyclic di-GMP (slower at higher concentration). The latter eventually activates the YcgR binding protein to interact like a molecular brake directly with the stator of the flagellar motor.[2b,c] Such fascinating modes of action have inspired chemists to design and investigate de novo artificial (supra)molecular devices and to control their function by external additives or inputs,[3] whereby multicomponent machinery[4] represents a particular challenge. We recently contributed to this area by developing the four-component supramolecular rotors ROT-1 and ROT-2 (Figure 1 B)[5] which exhibit a rotational frequency of 97 and 81 kHz, respectively, at room temperature. Thus, first examples impressively demonstrate new properties in supramolecular heteroaggregates.[4] The key challenge of the near future is thus to establish novel functions in further machines and to control their action or motion by external stimuli.[4d]

Herein, we will present a small series of new five-component nanorotors ROT-3 (Figure 1) whose rotational frequency can be adjusted between 38 and 5 kHz through variation of the fifth component (**1**–**6**). Components **1**–**6** set up side rotors that, according to the following data, act as brakes mimicking speed regulation in the bacterial flagellar motor.[2b,c] Moreover, the rotational frequency in ROT-3 = [(ROT-2)(**1**–**6**)$_2$] is quantitatively predictable on the basis of "conformational slippage". The model describes the braking effect of two orthogonal side rotors on the main rotor and thus a new mechanism in the molecular sciences. Although, the past decade has been distinguished by a plethora of reports[3] describing molecular devices based on rotational[6,7] and translational[8] motion, control of speed through braking interactions has been achieved usually in only rather small covalent systems.[7e,9,10]

For the present study it is important to understand the modus operandi of our recently described nanorotors[5a] ROT-1 = [Cu$_2$(**7**)(**8**)(DABCO)]$^{2+}$ and ROT-2 = [Cu$_4$(**7**)(**8**)-(DABCO)]$^{4+}$ operating via thermally activated leaps. Both rotors are hetero-zinc(II)porphyrin sandwich structures composed of stator **7** and rotator (= rotor blade) **8** that are linked by DABCO (= axle) and by copper(I) complexation. The thermally activated rotation begins with the rate-limiting endergonic departure of the pyridine/pyrimidine terminals of rotator **8** from the Cu$^+$-loaded phenanthroline stations of stator **7** and thus the separation of the heteroleptic pyridine and phenanthroline (HETPYP)[11] coordination bonds. In ROT-2, only two out of the four copper(I) phenanthroline stations of stator **7** are occupied at a given time by binding to the rotator's termini. As a result, addition of two equivalents of additives **1**–**6** will afford the new five-component nanorotors ROT-3 = [(ROT-2)(additive)$_2$] via HETPHEN[12] complexation (Figure 1 C). Typically, HETPHEN complexes ($\log K = 4.92 \pm 0.19$ for [Cu(phenAr$_2$)]$^+$ + phen, see Figure S20 in the Supporting Information (SI)) are ca. 50 times more stable than HETPYP[11] complexes ($\log K = 3.2 \pm 0.6$ for [Cu(phenAr$_2$)]$^+$ + py). Thus, any HETPHEN dissociation is unlikely to occur during rotary oscillations in ROT-3. There are different rotary leaps, though, in ROT-2 (mixed 90/180° leaps)[5a] and in ROT-1 and ROT-3 (pure 180° oscillations).

Synthesis of the nanorotors: Six different additives (Figure 1 A) were used as the fifth component in nanorotors ROT-3. All ROT-3 are fully characterized by ^{1}H NMR, ^{1}H-^{1}H COSY, ^{1}H DOSY, ESI-MS, and elemental analysis (see SI). When 2 equiv of additive **1** was mixed with the four-component nanorotor ROT-2[5a] in CD_2Cl_2:$CDCl_3$ = 9:1, we obtained quantitatively [Cu$_4$(**1**)$_2$(**7**)(**8**)(DABCO)]$^{4+}$ = [(ROT-2)(**1**)$_2$] = ROT-3,**1** (the second number refers to the additive, here **1**) as judged by ^{1}H NMR, ^{1}H-^{1}H COSY, and ESI-MS data. The ^{1}H NMR spectrum of ROT-3,**1** displays two

[*] Dr. S. K. Samanta,[+] M. Sc. A. Rana,[+] Prof. Dr. M. Schmittel
Center of Micro- and Nanochemistry and Engineering
Organische Chemie I, Universität Siegen
Adolf-Reichwein-Strasse 2, 57068 Siegen (Germany)
E-mail: schmittel@chemie.uni-siegen.de

[+] These authors contributed equally to this work.

Supporting information and ORCID(s) from the author(s) for this article are available on the WWW under http://dx.doi.org/10.1002/anie.201509108.

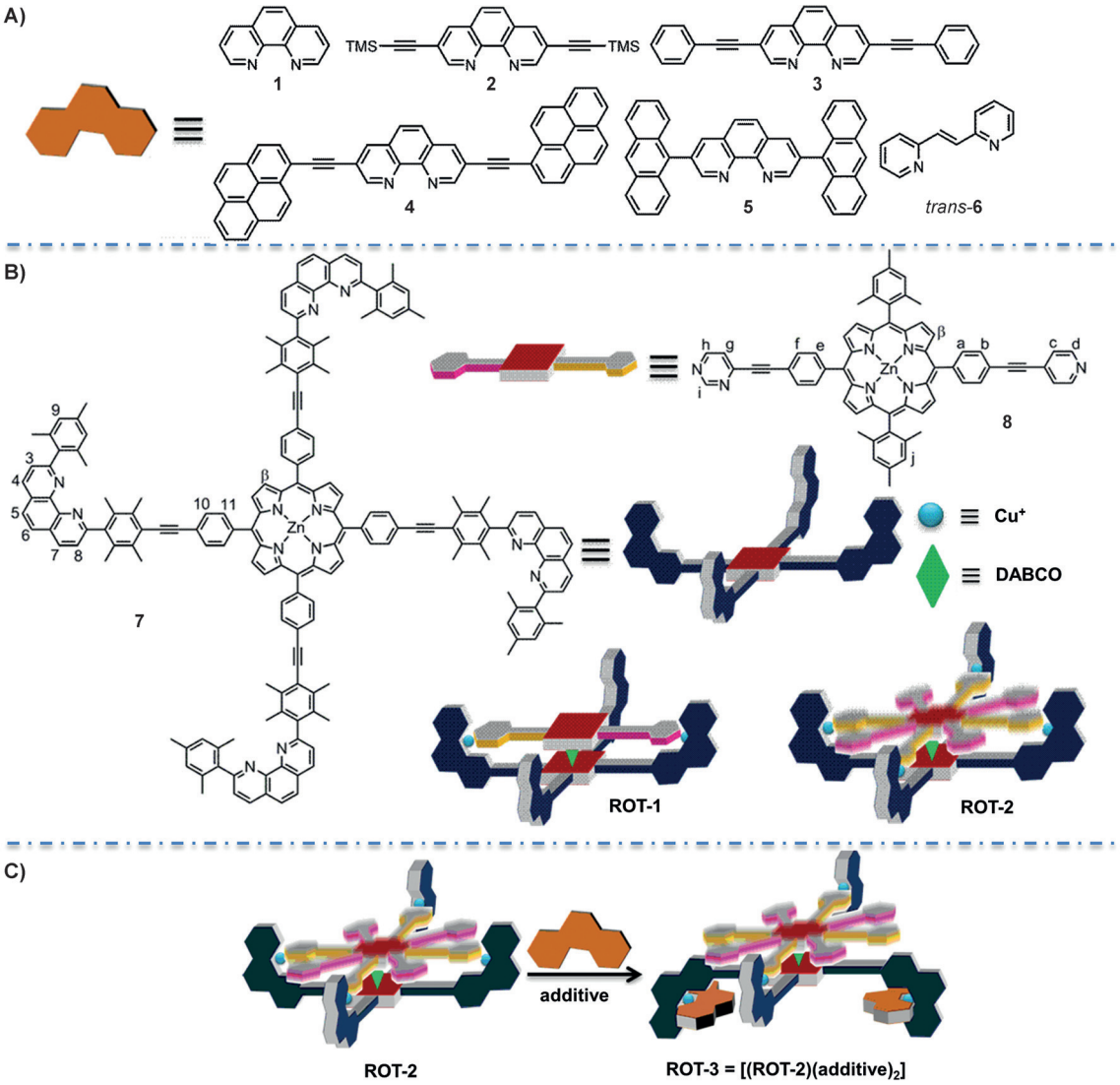

Figure 1. A) Additives **1**–**6** as brake blocks. B) Stator **7**, rotator **8** and the two known nanorotors ROT-1 and ROT-2 used as reference compounds. C) General procedure to synthesize the five-component nanorotors ROT-3.

diagnostic peaks (1:1) for protons 9-H at 7.10 and 6.00 ppm (Figure 2) showing the phenanthroline stations to be involved in HETPYP[11] and HETPHEN[12] complexation, respectively. The ESI mass spectrum displays two peaks at 1044.5 and 1441.7 Da corresponding to ions after loss of four (→ $[Cu_4(\mathbf{1})_2(\mathbf{7})(\mathbf{8})(DABCO)]^{4+}$) and three PF_6^- anions (→ $[Cu_4(\mathbf{1})_2(\mathbf{7})(\mathbf{8})(DABCO)](PF_6)^{3+}$), respectively (Figure 3 A). Finally, the ^{1}H DOSY spectrum showed ROT-3,**1** to be a single species in solution.

Frequency of rotation: Insight into the dynamics of spinning in ROT-3,**1** is obtained by variable-temperature (VT) ^{1}H NMR spectroscopy. While at 25 °C the mesityl protons 9-H of both phenanthroline stations that are involved in HETPYP complexation exhibit a single signal at $\delta = 7.10$ ppm indicative of fast exchange, the NMR spectrum at −75 °C displays two singlets of equal intensities at $\delta = 7.10$ and 7.07 ppm (Figure 3 B). The splitting arises as the two Cu^+-loaded phenanthroline stations are no longer degenerate since they are either coordinated to the pyridine or pyrimidine terminus of the unsymmetric rotator **8**. Reciprocally, as the temperature is increased, the two

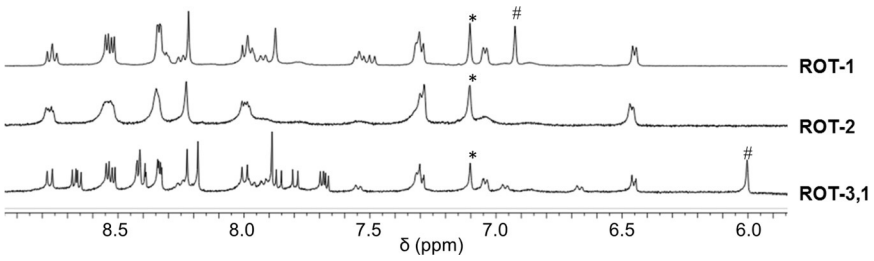

Figure 2. Partial ^{1}H NMR spectra of ROT-1, ROT-2, and ROT-3,**1** in CD_2Cl_2 at 25 °C (*: protons 9-H of the stator's phenanthroline ligands involved in HETPYP complexation. #: 9-H of Cu^+-free phenanthroline sites in ROT-1 and of phenanthroline ligands involved in HETPHEN complexation in ROT-3,**1**, respectively).

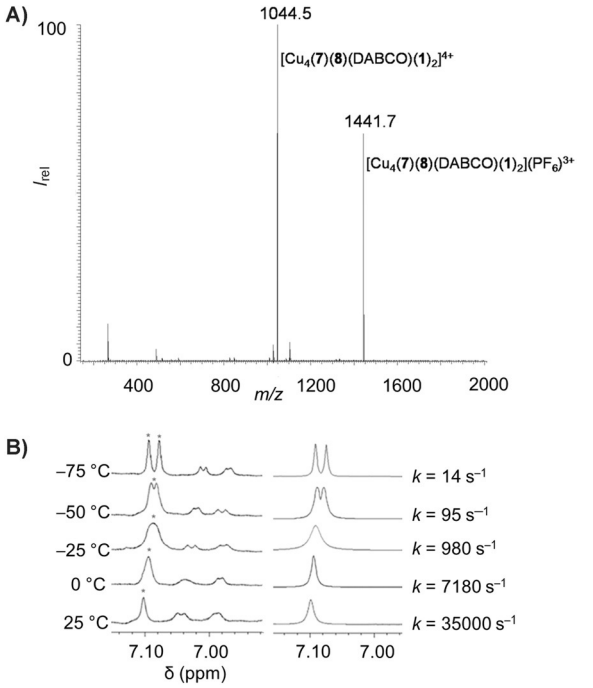

Figure 3. Spectra of ROT-3,**1**. A) ESI-MS in CD_2Cl_2. B) VT ^1H NMR (600 MHz) in CD_2Cl_2 (left: experimental; right: simulated).

peaks gradually broaden, then coalesce, and finally at 25 °C form a sharp singlet ($\delta = 7.10$ ppm).[13] The rotational frequency at 25 °C (k_{25}) in the five-component nanorotor ROT-3,**1** is determined to be $k_{25} = 35\,000\ s^{-1}$, which is much lower than that in the four-component 180° nanorotor ROT-1 ($k_{25} = 97\,000\ s^{-1}$).[5a] Replacement of **1** by other additives, that is, **2**–**5**, adjusts the speed (k_{25}) over a wide range (Table 1).

Table 1: Computed dihedral contact angle (ϕ_c), number of non-interfering conformations (n), slippage constant (ζ), and experimental vs. calculated rotational frequencies at 25 °C for ROT-3.

Rotor	ϕ_c[a]	ζ (n)[b]	Expt. rotational frequency [s^{-1}]	Calcd. rotational frequency[c] [s^{-1}]
ROT-3,**1**	±109°	0.36 (47089)	35 000 ± 920	35 200
ROT-3,**2**	±70°	0.15 (19321)	19 080 ± 670	14 500
ROT-3,**3**	±74°	0.17 (21 609)	18 300 ± 490	16 200
ROT-3,**4**	±41°	0.05 (6561)	5700 ± 180	4900
ROT-3,**5**	±37°	0.04 (5329)	4900 ± 140	4000

[a] Calculated using PM6, see text. [b] $\zeta = (n/129\,600)$. 129 600 is the number of all possible conformations. [c] Calculated as follows: $k_{25} = \zeta \times 97\,000\ s^{-1}$. ROT-1 ($k_{25} = 97\,000\ s^{-1}$) serves as a reference for a pure 180° nanorotor.

Noticeably the rate-determining step in ROT-3 is no longer controlled by the departure of the rotator from the copper-loaded stations as in ROT-1, but by a completely different mechanism.

Braking mechanism: All four phenanthroline sites in stator **7** and thus in rotors ROT-3 are actually rotors themselves, here referred to as side rotors, because their alkynyl linkage to the porphyrin exhibits a low rotational barrier.[14] Molecular modeling studies indicate that depending on their conformational orientation the bulky HETPHEN side rotors in ROT-3, that is, the phenanthroline sites loaded with brake blocks **1**–**5**, interfere with the trajectory of the main rotator (Figure 4 A). Clearly, obstruction of the main rotator's trajectory by a single HETPHEN side rotor should already block rotation, as illustrated in the conformation ROT-3^{II} (Figure 4 C).

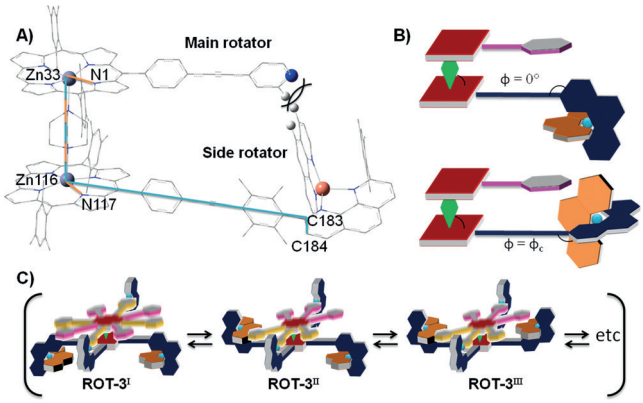

Figure 4. A) Partial structure of ROT-3,**1** as used in the PM6 computations. Only the interfering hydrogen atoms of the main and side rotator at the contact angle ϕ_c are highlighted. B) Cartoon representation of this partial structure at $\phi = 0°$ and at the angle ϕ_c. C) Three selected conformations of ROT-3 (ROT-3^I, ROT-3^{II}, and ROT-3^{III}).

To rationalize speed deceleration in ROT-3, we considered four mechanistic scenarios: 1) gearing, 2) solid-disk interference (i.e., the fast HETPHEN side rotors generate a "solid disk-shaped object" in the trajectory of the main rotator), 3) passage through open conformations, and 4) conformational slippage.

Regarding mechanism (1), we consider normal gearing as unlikely because side and main rotors should operate at different rates (vide infra). Moreover, since only a one-touch gearing would apply, the deceleration should not be highly dependent on the lateral extension of the additive. Thus one would expect similar rates for ROT-3 with additives **2**–**4**, which is not the case.

Considering their sub-picosecond time scale for rotation, the HETPHEN side rotors may be described as solid disk objects in the trajectory of the main rotator (scenario 2) requiring strong bending of the rotator about the disk-like object to avoid interference. Obviously, the larger the radius of the solid disk object, the slower the rotational frequency of the main rotor. An assessment of the side rotators' radii in ROT-3 by conformational analysis using PM6 (Figure S30) predicts the following relative rotational speed: **1** ($r = 8.2$ Å) > **5** (10.0 Å) > **2** (11.1 Å) > **3** (12.8 Å) ≫ **4** (16.6 Å) quite in contrast to the experimental data for k_{25}: **1** > **2**,**3** > **4**,**5**.

Hypothesis (3) claims that the ratio of obstructing and non-obstructing conformations dictates the passage of the main rotator through the rotating side rotors of ROT-3. For this purpose, the main rotor obviously has to have a significantly higher speed than the side rotor in the moment of the passage, which can be ruled out based on the low rotational barrier of the HETPHEN side rotor (2 kJ mol^{-1}; PM6).[15] Equally, based on classical mechanical considerations (see SI)

the main rotor should be decisively slower than the HETPHEN side rotors.

As a result of the failure of the hypotheses (1)–(3) we suggest a new model (4), called conformational slippage, which is inspired by mechanism (3). This model presumes that the "diffusive" encounter of the two rotators results initially in an adjustment of their speeds before the main rotator is able to slip to the other side, depending on the extent of conformational aperture.

In the unimpeded rotor ROT-1 the Gibbs energy changes are best represented by the gray profile in Figure 5A. At the

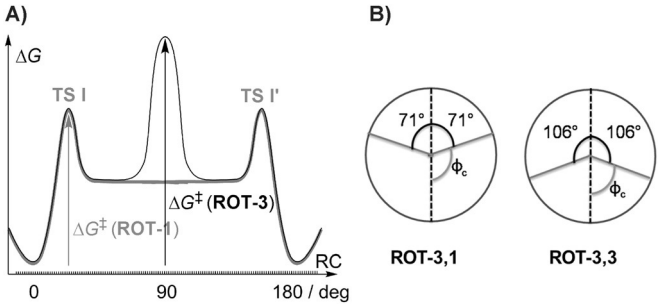

Figure 5. A) Schematic Gibbs energy profile of the rotation in ROT-1 (gray) and ROT-3 (black). B) Pictorial representation of the conformational situation at the HETPHEN side rotor in ROT-3 depending on the additives (brake blocks). The larger the cut-off angle (ϕ_c), the fewer the number of interfering conformations.

point at which the pyridine and pyrimidine terminals of the rotator arm detach from the copper-loaded phenanthroline stations, the rate-determining reaction barrier (TS I) is reached. On the ensuing rather shallow local minimum, the main rotator should easily pass from one side (Figure 5A, $<90°$) to the other ($>90°$). In contrast, the rate-determining barrier in ROT-3 is generated by the encounter of main and side rotator at ca. 90°.

Let us visualize the encounter of the two rotators each operating at a different speed with the HETPHEN side rotor being the faster one (vide supra). As a result, the main rotator arm is reflected and oscillates back and forth in its local minimum. During those "diffusive" encounters both rotors may lose velocity, until they assume the same speed. Only now, the main rotator may find a passage through the side rotor depending on the number of unobstructing conformations (conformational slippage).

In order to assess conformational slippage in relation to that in the unhindered 180° nanorotor ROT-1 (97000 s^{-1}),[5a] we simply determined the ratio of noninterfering conformations to the total number of conformations. For example, in conformer ROT-3^{I} both side rotators are directed away ($\phi_{Zn33\text{-}Zn116\text{-}C183\text{-}C184} = 0°$) from the trajectory of the main rotator and thus allow uninhibited rotation (Figure 4C). Conversely, in ROT-3^{II} and ROT-3^{III} either one or both side rotators should protrude into the main rotator's path ($\phi_{Zn33\text{-}Zn116\text{-}C183\text{-}C184} = \pm 180°$) thus strongly impeding its rotation. Our model now assumes that the main rotator is able to slip "diffusively" to the other side depending on the proportion of unobstructed conformations.

Fortunately, conformational slippage can be assessed quantitatively by calculating the unobstructing vs. obstructing conformations. At first, the steric interaction during the encounter of the two rotators (depending on the angle ϕ) is determined using single-point PM6 computations. Upon contact the calculated energy sharply rises, which allows the definition of a contact dihedral angle ϕ_c (Figure 6A).[16] All

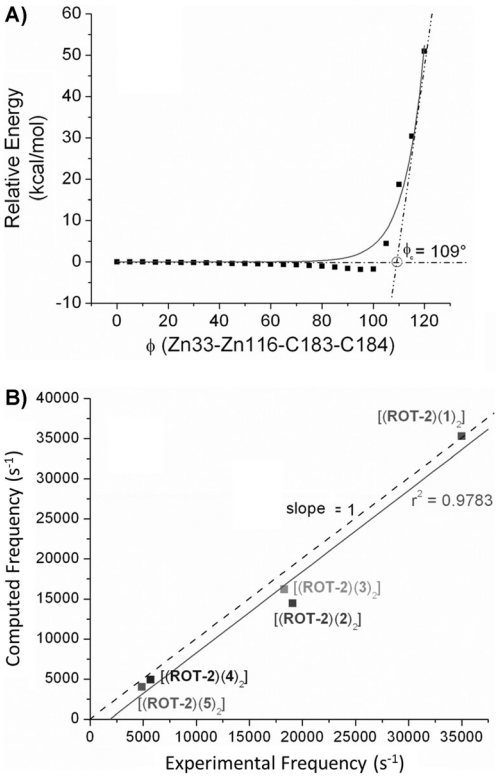

Figure 6. A) Relative energy of ROT-3,**1** as a function of the dihedral angle ϕ of the side rotator as obtained from single-point PM6 computations (dihedral angle N1-Zn33-Zn116-N117 of the main rotator = 25°).[19] B) Experimental vs. computed rotational frequency for all rotors. The solid line represents the linear regression obtained by applying the conformational slippage model while, for comparison, the dashed line corresponds to the ideal 1:1 correlation.

conformers between $180° \geq |\phi|$ (side rotator) $\geq |\phi_c|$ are considered to interfere with the main rotator's passage while the others are noninterfering. Based on this angle, the total conformational space of 129600 independent conformations (360×360, 1 deg steps) may be split into interfering and noninterfering conformations.

For instance, PM6 computations furnished an angle $\phi_c = \pm 109°$ for ROT-3,**1** (Figure 6A, Table 1). Thus, all conformations of the side rotators with an angle $|\phi|$ between 0° and 109° should allow passage of the main rotator (Figure 5B). Noticeably, the other ROT-3 rotors exhibit vastly different ϕ_c values (Table 1) due to the differently sized additives.

The larger the angle ϕ_c, the greater the proportion of noninterfering conformations and thus the higher the rotational speed. In the case of ROT-3,**1**, a $\phi_c = \pm 109°$ indicates that 82511 out of 129600 conformers, that is, 64%, prevent passage of the spinning main rotator (for details of this

calculation, see Section 7 of the Supporting Information), while 36% do not interfere with the trajectory. Hence, the rotational frequency is calculated as $k_{25} = \zeta \times 97000\ s^{-1} = 0.36 \times 97000\ s^{-1} = 35200\ s^{-1}$, quite close to the experimental value of $35000\ s^{-1}$ (Table 1). Also for the other nanorotors ROT-3, this model predicts rotational frequencies that agree rather well with the experimental data (Table 1, Figure 6B).

Reversible speed regulation in an in situ prepared nanorotor has been realized recently by using **6** as the fifth component.[17] It was shown that photochemical *trans–cis* isomerization of **6** led to rotor ROT-3,**6** = [(ROT-2)(*cis*-**6**)$_2$], the rotational frequency of which at 25 °C was experimentally determined as $38200\ s^{-1}$.[5b] Using the above presented model on conformational slippage, the frequency is calculated to $37200\ s^{-1}$ which is in convincing agreement with the determined experimental data.

The strong decrease of the rotational frequency in ROT-3,**4** and ROT-3,**5** raises concern about the integrity of the assembly as the activation barrier increases. However, even with the slowest rotor, ROT-3,**5**, the barrier of 52.3 kJ mol^{-1} is more than 9.6 kJ mol^{-1} lower than the lower limit for dissociation/association ($\Delta G_{25}^{\neq} = 61.9$ kJ mol^{-1}).[18] Thus, far more than 98% of the rotary motion will follow the intrasupramolecular spinning pathway. Actually, the finding of speed regulation in ROT-3 is compelling evidence for intrasupramolecular spinning as the dissociative/associative mechanism should not respond to the size of the additive(s).

In conclusion, a series of self-assembled five-component nanorotors have been prepared and their rotational frequencies measured. Depending on the size of the brake blocks, the frequency of the main rotor has values between 35 and 5 kHz. The model we developed to explain these results, conformational slippage, is based on classical mechanics and proved to be reliable in predicting the rotational frequency in our nanorotors. To the best of our knowledge, the modus operandi is unprecedented in (supra)molecular machinery and possibly could be of importance for flagellar motors.[2b,c]

Acknowledgements

We are indebted to the DFG (Schm 647/20-1) and the Universität Siegen for financial support.

Keywords: coordination chemistry · NMR spectroscopy · rate regulation · rotation · supramolecular chemistry

How to cite: *Angew. Chem. Int. Ed.* **2016**, *55*, 2267–2272
Angew. Chem. **2016**, *128*, 2309–2314

[1] a) S. Rice, A. W. Lin, D. Safer, C. L. Hart, N. Naber, B. O. Carragher, S. M. Cain, E. Pechatnikova, E. M. Wilson-Kubalek, M. Whittaker, E. Pate, R. Cooke, E. W. Taylor, R. A. Milligan, R. D. Vale, *Nature* **1999**, *402*, 778; b) M. Yoshida, E. Muneyuki, T. Hisabori, *Nat. Rev. Mol. Cell Biol.* **2001**, *2*, 669; c) M. Schliwa, G. Woehlke, *Nature* **2003**, *422*, 759; d) R. Dreyfus, J. Baudry, M. L. Roper, M. Fermigier, H. A. Stone, J. Bibette, *Nature* **2005**, *437*, 862.

[2] a) J. P. Armitage, R. M. Berry, *Cell* **2010**, *141*, 24; b) A. Boehm, M. Kaiser, H. Li, C. Spangler, C. A. Kasper, M. Ackermann, V. Kaever, V. Sourjik, V. Roth, U. Jenal, *Cell* **2010**, *141*, 107; c) K. Paul, V. Nieto, W. C. Carlquist, D. F. Blair, R. M. Harshey, *Mol. Cell* **2010**, *38*, 128.

[3] a) G. S. Kottas, L. I. Clarke, D. Horinek, J. Michl, *Chem. Rev.* **2005**, *105*, 1281; b) E. R. Kay, D. A. Leigh, F. Zerbetto, *Angew. Chem. Int. Ed.* **2007**, *46*, 72; *Angew. Chem.* **2007**, *119*, 72; c) *From Non-Covalent Assemblies to Molecular Machines* (Eds.: J.-P. Sauvage, P. Gaspard), Wiley-VCH, Weinheim, **2010**; d) U. Lüning, *Angew. Chem. Int. Ed.* **2012**, *51*, 8163; *Angew. Chem.* **2012**, *124*, 8285; e) C. Fasting, C. A. Schalley, M. Weber, O. Seitz, S. Hecht, B. Koksch, J. Dernedde, C. Graf, E.-W. Knapp, R. Haag, *Angew. Chem. Int. Ed.* **2012**, *51*, 10472; *Angew. Chem.* **2012**, *124*, 10622; f) C. Kremer, A. Lützen, *Chem. Eur. J.* **2013**, *19*, 6162; g) S. De, S. Pramanik, M. Schmittel, *Angew. Chem. Int. Ed.* **2014**, *53*, 14255; *Angew. Chem.* **2014**, *126*, 14480; h) G. Haberhauer, C. Burkhart, S. Woitschetzki, C. Wölper, *J. Org. Chem.* **2015**, *80*, 1887.

[4] a) R. Hernandez, H.-R. Tseng, J. W. Wong, J. F. Stoddart, J. I. Zink, *J. Am. Chem. Soc.* **2004**, *126*, 3370; b) H. Kai, S. Nara, K. Kinbara, T. Aida, *J. Am. Chem. Soc.* **2008**, *130*, 6725; c) S. V. Bhosale, C. Chong, C. Forsyth, S. J. Langford, C. P. Woodward, *Tetrahedron* **2008**, *64*, 8394; d) S. Hiraoka, E. Okuno, T. Tanaka, M. Shiro, M. Shionoya, *J. Am. Chem. Soc.* **2008**, *130*, 9089; e) S. Hiraoka, Y. Hisanaga, M. Shiro, M. Shionoya, *Angew. Chem. Int. Ed.* **2010**, *49*, 1669; *Angew. Chem.* **2010**, *122*, 1713; f) M. Nishikawa, K. Nomoto, S. Kume, H. Nishihara, *J. Am. Chem. Soc.* **2012**, *134*, 10543; g) Q.-C. Zhang, F.-T. Wu, H.-M. Hao, H. Xu, H.-X. Zhao, L.-S. Long, R.-B. Huang, L.-S. Zheng, *Angew. Chem. Int. Ed.* **2013**, *52*, 12602; *Angew. Chem.* **2013**, *125*, 12834; h) S. Liu, D. V. Kondratuk, S. A. L. Rousseaux, G. Gil-Ramírez, M. C. O'Sullivan, J. Cremers, T. D. W. Claridge, H. L. Anderson, *Angew. Chem. Int. Ed.* **2015**, *54*, 5355; *Angew. Chem.* **2015**, *127*, 5445; i) T. R. Cook, P. J. Stang, *Chem. Rev.* **2015**, *115*, 7001; j) A. J. McConnell, C. S. Wood, P. P. Neelakandan, J. R. Nitschke, *Chem. Rev.* **2015**, *115*, 7729.

[5] a) S. K. Samanta, M. Schmittel, *J. Am. Chem. Soc.* **2013**, *135*, 18794; b) S. K. Samanta, J. W. Bats, M. Schmittel, *Chem. Commun.* **2014**, *50*, 2364.

[6] a) G. Haberhauer, *Angew. Chem. Int. Ed.* **2011**, *50*, 6415; *Angew. Chem.* **2011**, *123*, 6539; b) J. Wang, B. L. Feringa, *Science* **2011**, *331*, 1429; c) T. Kudernac, N. Ruangsupapichat, M. Parschau, B. Macía, N. Katsonis, S. R. Harutyunyan, K.-H. Ernst, B. L. Feringa, *Nature* **2011**, *479*, 208; d) A. Guenet, E. Graf, N. Kyritsakas, M. W. Hosseini, *Chem. Eur. J.* **2011**, *17*, 6443; e) B. E. Dial, R. D. Rasberry, B. N. Bullock, M. D. Smith, P. J. Pellechia, S. Profeta, K. D. Shimizu, *Org. Lett.* **2011**, *13*, 244; f) M. Nishikawa, S. Kume, H. Nishihara, *Phys. Chem. Chem. Phys.* **2013**, *15*, 10549.

[7] Selected papers: a) N. Zigon, P. Larpent, A. Jouaiti, N. Kyritsakas, M. W. Hosseini, *Dalton Trans.* **2014**, *43*, 15779; b) C.-Y. Kao, H.-F. Lu, I. Chao, J.-S. Yang, *Org. Lett.* **2014**, *16*, 6100; c) L. Greb, J.-M. Lehn, *J. Am. Chem. Soc.* **2014**, *136*, 13114; d) K. Zhao, P. I. Dron, J. Kaleta, C. T. Rogers, J. Michl, *Top. Curr. Chem.* **2014**, *354*, 163; e) P. Commins, M. A. Garcia-Garibay, *J. Org. Chem.* **2014**, *79*, 1611.

[8] a) J. D. Badjić, V. Balzani, A. Credi, S. Silvi, J. F. Stoddart, *Science* **2004**, *303*, 1845; b) B. K. Juluri, A. S. Kumar, Y. Liu, T. Ye, Y.-W. Yang, A. H. Flood, L. Fang, J. F. Stoddart, P. S. Weiss, T. J. Huang, *ACS Nano* **2009**, *3*, 291; c) J.-P. Collin, F. Durola, J. Lux, J.-P. Sauvage, *Angew. Chem. Int. Ed.* **2009**, *48*, 8532; *Angew. Chem.* **2009**, *121*, 8684; d) A. Carlone, S. M. Goldup, N. Lebrasseur, D. A. Leigh, A. Wilson, *J. Am. Chem. Soc.* **2012**, *134*, 8321; e) B. Lewandowski, G. De Bo, J. W. Ward, M. Papmeyer, S. Kuschel, M. J. Aldegunde, P. M. E. Gramlich, D. Heckmann, S. M. Goldup, D. M. D'Souza, A. E. Fernandes, D. A. Leigh, *Science* **2013**, *339*, 189; f) C. Talotta, C. Gaeta, Z. Qi, C. A. Schalley, P. Neri, *Angew. Chem. Int. Ed.* **2013**, *52*, 7437;

Angew. Chem. **2013**, *125*, 7585; g) C. J. Bruns, J. F. Stoddart, *Acc. Chem. Res.* **2014**, *47*, 2186; h) T. Heinrich, C. H.-H. Traulsen, M. Holzweber, S. Richter, V. Kunz, S. K. Kastner, S. O. Krabbenborg, J. Huskens, W. E. S. Unger, C. A. Schalley, *J. Am. Chem. Soc.* **2015**, *137*, 4382.

[9] T. R. Kelly, M. C. Bowyer, K. V. Bhaskar, D. Bebbington, A. Garcia, F. Lang, M. H. Kim, M. P. Jette, *J. Am. Chem. Soc.* **1994**, *116*, 3657.

[10] a) M. C. Basheer, Y. Oka, M. Mathews, N. Tamaoki, *Chem. Eur. J.* **2010**, *16*, 3489; b) S. Ogi, T. Ikeda, R. Wakabayashi, S. Shinkai, M. Takeuchi, *Chem. Eur. J.* **2010**, *16*, 8285; c) W.-T. Sun, Y.-T. Huang, G.-J. Huang, H.-F. Lu, I. Chao, S.-L. Huang, S.-J. Huang, Y.-C. Lin, J.-H. Ho, J.-S. Yang, *Chem. Eur. J.* **2010**, *16*, 11594; d) D. K. Frantz, A. Linden, K. K. Baldridge, J. S. Siegel, *J. Am. Chem. Soc.* **2012**, *134*, 1528; e) B. E. Dial, P. J. Pellechia, M. D. Smith, K. D. Shimizu, *J. Am. Chem. Soc.* **2012**, *134*, 3675; f) N. Zigon, A. Guenet, E. Graf, N. Kyritsakas, M. W. Hosseini, *Dalton Trans.* **2013**, *42*, 9740; g) W.-T. Sun, G.-J. Huang, S.-L. Huang, Y.-C. Lin, J.-S. Yang, *J. Org. Chem.* **2014**, *79*, 6321.

[11] HETPYP = HETeroleptic PYridine- and Phenanthroline-complexes. In the break-up of a HETPYP complexation motif $[Cu(phen)(py)]^+ \rightarrow [Cu(phen)]^+ + py$ usually the weaker binding pyridine (py) is separated from the copper phenanthroline complex $[Cu(phen)]^+$. a) S. K. Samanta, D. Samanta, J. W. Bats, M. Schmittel, *J. Org. Chem.* **2011**, *76*, 7466; b) S. Neogi, G. Schnakenburg, Y. Lorenz, M. Engeser, M. Schmittel, *Inorg. Chem.* **2012**, *51*, 10832.

[12] HETPHEN = HETeroleptic BisPHENanthroline Complexes. The HETPHEN strategy allows the defined preparation of heteroleptic $[Cu(phen1)(phen2)]^+$ bisphenanthroline complexes. a) M. Schmittel, A. Ganz, *Chem. Commun.* **1997**, 999; b) M. Schmittel, H. Ammon, V. Kalsani, A. Wiegrefe, C. Michel, *Chem. Commun.* **2002**, 2566; c) R. S. K. Kishore, T. Paululat, M. Schmittel, *Chem. Eur. J.* **2006**, *12*, 8136; d) M. Schmittel, S. De, S. Pramanik, *Angew. Chem. Int. Ed.* **2012**, *51*, 3832; *Angew. Chem.* **2012**, *124*, 3898; e) S. Pramanik, S. De, M. Schmittel, *Angew. Chem. Int. Ed.* **2014**, *53*, 4709; *Angew. Chem.* **2014**, *126*, 4798.

[13] T. Kajiwara, S. Yokozawa, T. Ito, N. Iki, N. Morohashi, S. Miyano, *Angew. Chem. Int. Ed.* **2002**, *41*, 2076; *Angew. Chem.* **2002**, *114*, 2180.

[14] A. R. Karim, A. Linden, K. K. Baldridge, J. S. Siegel, *Chem. Sci.* **2010**, *1*, 102.

[15] J. J. P. Stewart, *J. Mol. Model.* **2007**, *13*, 1173.

[16] The contact dihedral angle ϕ_c is determined from the intersection point of the two tangents drawn from the energy profile curve.

[17] In contrast to the other nanorotors ROT-3, ROT-3,**6** was not isolated because it was prepared in presence of excess of *trans*-**6**, see Ref. [5b]. The nanorotors ROT-3,**1-5** are thus the first fully characterized five-component machines.

[18] The dissociation/association thermodynamics (61.9 kJ mol^{-1}, see Ref. [5a]) does not include any cooperative effects.

[19] The rotational energy profile about the HETPHEN side rotators was computed using PM6 in Gaussian 09 with the main rotator being fixed at a dihedral angle of 25° about N1-Zn33-Zn116-N117, as this angle allowed maximum interference. Single-point energy data were calculated because adaptive maneuvers by coupled conformational changes of the rotators at the moment of encounter are not envisaged by the model.

Received: September 29, 2015
Published online: January 6, 2016

